Electronic Supplementary Material (ESI) for Materials Chemistry Frontiers.

Supporting Information

Acceptor Modulation for Blue and Yellow TADF Materials and Fabrication of All-TADF White OLED

Ruizhi Dong,[a] Di Liu,*[a,b] Jiuyan Li,*[a] Mengyao Ma,[a] Yongqiang Mei,[a] Deli Li[a]

Jingyang Jiang[a]

[a] State Key Laboratory of Fine Chemicals, School of Chemical Engineering, Dalian University of Technology, 2 Linggong Road, Dalian, 116024, China.

E-mail: liudi@dlut.edu.cn, jiuyanli@dlut.edu.cn

[b] State Key Laboratory of Luminescent Materials and Devices, South China University of Technology, Guangzhou, 510640, China.

Experimental Section

General information

All reagents are purchased from commercial sources and used without further purification. The ^{1}H NMR and ^{13}C NMR spectra were recorded using a 400 MHz, 500 MHz and 126 MHz Varian Unity Inova spectrophotometer. The mass spectra were recorded on a HP1100LC/MSD MS spectrometer. The phosphorescence spectra were measured in 2-MeTHF glass matrix at 77 K using a Hitachi F-4600 fluorescence spectrometer. The fluorescence and UV-vis absorption spectra measurements were performed on a Perkin-Elmer LS55 spectrometer and a Perkin-Elmer Lambda 35 spectrophotometer, respectively. Temperature dependent transient PL spectra were measured with an Edinburgh FLS1000 fluorescence spectrophotometer. Temperature transient PL decay was measured with an Edinburgh FLS1000 fluorescence spectrophotometer. Thermogravimetric analyses (TGA) was performed on a Perkin-Elmer thermogravimeter (Model TGA7) under a N_2 flow at a heating rate of 10 ℃ min^{-1}. DSC measurements were operated on a Netzsch DSC 201 under a N_2 flow at a heating rate of 10 ℃ min^{-1} and cooling by liquid nitrogen. Cyclic voltammograms (CV) were recorded using a conventional three electrode configuration and an electrochemical workstation (CHI610E) at a scan rate of 100 mV s^{-1}. A glass carbon working electrode, a Pt-wire counter electrode, and a saturated calomel electrode (SCE) reference electrode were used. All the measurements were made at room temperature on deoxygenated samples in dichloromethane with 0.1 M tetrabutylammonium hexafluorophosphate (*n*-Bu_4NPF_6) as the electrolyte.

OLED Fabrication and Measurements

Before device fabrication, the ITO glass substrates with a sheet resistance of 10~15 Ω per square were carefully pre-cleaned, and then treated by UV-ozone for 30 min. A 40 nm thick PEDOT:PSS film was spin coated on the ITO glass substrate firstly and baked at 120 ℃ for 30 min in air. Subsequently, the substrate was transferred into a vacuum chamber to deposit the organic layers with a base pressure of less than 10^{-6} Torr (1 Torr =133.32 Pa). A 1 nm thin layer of LiF and subsequently a 200 nm thin layer of Al were vacuum deposited as the cathode. Deposition rates are 0.1 Å s^{-1} for LiF and 6 Å s^{-1} for Al. The emitting area of each pixel was determined by the overlapping of the two electrodes as 9 mm^2. The *J–V–B* curves of the devices were measured with a Konica Minolta CS200 photometer and a source-measure-unit Keithley 2400 under ambient conditions at room temperature, then, the EL spectra and CIE coordinates of the devices were measured with a PR705 photometer and a source-measure-unit Keithley 236 under ambient conditions at room temperature. The forward viewing external quantum efficiency was calculated by using the current efficiency, EL spectra and human photopic sensitivity.

Compound syntheses

Synthesis of 4,4'-(4-chloropyridine-2,6-diyl)dibenzonitrile (1). To a deoxygenated solution containing 2,4,6-trichloropyridine (224 mg, 1 mmol), 4-cyanophenylboronic acid (900 mg, 2mmol), toluene (15 mL), ethanol (3 mL), and aqueous sodium carbonate (2 M, 4 mL, 8 mmol) was added tetrakis(triphenylphosphino)palladium(0) (120 mg, 0.1 mmol) under nitrogen

atmosphere. The reaction mixture was refluxed for 12 hours. After cooling to room temperature and diluted by water (10 mL), the organic layer was separated and the aqueous layer was extracted with dichloromethane (3 × 15 mL). The combined organic layers were dried over anhydrous magnesium sulfate and filtered. The crude product was purified by column chromatography over silica using dichloromethane:petroleum mixture (1:1) as eluent to yield the pure product as white solid (106 mg, yield 60%). MALDI-TOF-MS (*m/z*): cal. for $C_{19}H_{10}ClN_3$ 315.0563; found, 315.0554 $[M]^+$.

Synthesis of 4,4'-(4-(4-chlorophenyl)pyridine-2,6-diyl)dibenzonitrile (2). To a deoxygenated solution containing (1) (450 mg, 1 mmol), (4-chlorophenyl)boronic acid (900 mg, 1mmol), toluene (15 mL), ethanol (3 mL), and aqueous sodium carbonate (2 M, 4 mL, 8 mmol) was added tetrakis(triphenylphosphino)palladium(0) (120 mg, 0.05 mmol) under nitrogen atmosphere. The reaction mixture was refluxed for 12 hours. After cooling to room temperature and diluted by water (10 mL), the organic layer was separated and the aqueous layer was extracted with dichloromethane (3 × 15 mL). The combined organic layers were dried over anhydrous magnesium sulfate and filtered. The crude product was purified by column chromatography over silica using dichloromethane:petroleum mixture (1:1) as eluent to yield the pure product as white solid (216 mg, yield 49%). MALDI-TOF-MS (*m/z*): cal. for $C_{25}H_{14}ClN_3$ 391.0876; found, 391.0866 $[M]^+$.

General procedure for synthesis of 4,4'-(4-(4-(10*H*-phenoxazin-10-yl)phenyl)pyridine-2,6-diyl)dibenzonitrile

(PyDCN-PXZ) and 4,4'-(4-(4-(9,9-dimethylacridin-10(9*H*)-yl)phenyl)pyridine-2,6-diyl)dibenzonitrile. (PyDCN-DMAC). The mixture of intermediate 2 (600 mg, 0.5 mmol), 10H-phenoxazine or 9,9-dimethyl-9,10-dihydro-acridine (0.5 mmol), $Pd_2(dba)_3$ (46 mg, 0.025 mmol), Cs_2CO_3 (652 mg, 1 mmol), and $(tBu)_3P \cdot HBF_4$ (16 mg, 0.025 mmol) was added to dehydrated toluene (40 mL). The mixture was stirring and refluxed for 24 h under argon atmosphere. After being cooled to room temperature, the resulting mixture was poured into water and extracted with dichloromethane three times. After the combined organic layers were dried over anhydrous magnesium sulfate and the solvent was removed under vacuum. Then the residue was purified by column chromatography with dichloromethane/petroleum ether (1:1) as an eluent and further purified by repeated recrystallization in methanol/chloroform to produce pure product.

PyDCN-PXZ: light yellow solid. Yield 46%. ^{1}H NMR (400 MHz, $CDCl_3$) δ: 8.34 (d, *J* = 7.7 Hz, 4H), 8.05 (s, 2H), 7.97 (d, *J* = 7.6 Hz, 2H), 7.85 (d, *J* = 7.6 Hz, 4H), 7.56 (d, *J* = 7.6 Hz, 2H), 6.77 – 6.59 (m, 6H), 6.00 (d, *J* = 7.4 Hz, 2H). ^{13}C NMR (126 MHz, $CDCl_3$) δ: 155.97, 150.19, 144.00, 142.90, 140.51, 138.18, 134.01, 132.69, 131.95, 129.90, 127.67, 123.26, 121.74, 118.68, 118.63, 115.70, 113.19, 113.07. MALDI-TOF-MS (*m/z*): cal. for $C_{37}H_{22}N_4O$ 538.1794; found, 538.1804 $[M]^+$. Anal. Calcad for $C_{37}H_{22}N_4O$: C, 82.51; H, 4.12; N, 10.40; Found: C, 82.49; H, 4.11; N, 10.40.

PyDCN-DMAC: greenish-yellow solid. Yield: 42%.^{1}H NMR (400 MHz, $CDCl_3$) δ: 8.36 (d, *J* = 7.4 Hz, 4H), 8.09 (d, *J* = 9.0 Hz, 2H), 8.01 (d, *J* = 7.4 Hz, 2H), 7.85 (d,

J = 7.6 Hz, 4H), 7.53 (dd, *J* = 21.8, 7.3 Hz, 4H), 6.99 (p, *J* = 7.0 Hz, 4H), 6.33 (d, *J* = 7.8 Hz, 2H), 1.72 (s, 6H).^{13}C NMR (126 MHz, $CDCl_3$) δ: 155.93, 150.37, 142.97, 142.79, 140.66, 137.91, 132.69, 132.42, 130.27, 129.75, 128.12, 127.71, 126.43, 125.47, 120.94, 118.71, 113.98, 113.03, 36.05, 31.33, 31.29. MALDI-TOF-MS (*m/z*): cal. for $C_{40}H_{28}N_4$ 564.2314; found, 564.2309 $[M]^+$. Anal. Calcad for $C_{40}H_{28}N_4$: C, 85.08; H, 5.00; N, 9.92; Found: C, 85.07; H, 5.01; N, 9.91.

Estimation of basic photophysical data

According to transient decay curves and photoluminescence quantum yield measurement, [1-3] we can obtain:

$$\Phi_{prompt} = \Phi_{PL} R_{prompt} \quad (1)$$

$$\Phi_{delayed} = \Phi_{PL} R_{delayed} \quad (2)$$

$$k_F = \Phi_{prompt}/\tau_{prompt} \quad (3)$$

$$\Phi_{PL} = k_F/(k_F + k_{IC}) \quad (4)$$

$$\Phi_{prompt} = k_F/(k_F + k_{IC} + k_{ISC}) \quad (5)$$

$$\Phi_{IC} = k_{IC}/(k_F + k_{IC} + k_{ISC}) \quad (6)$$

$$\Phi_{ISC} = k_{ISC}/(k_F + k_{IC} + k_{ISC}) = 1 - \Phi_{prompt} - \Phi_{IC} \quad (7)$$

$$\Phi_{RISC} = \Phi_{delayed}/\Phi_{ISC} \quad (8)$$

$$k_{RISC} = (k_p k_d \Phi_{delayed})/(k_{ISC} \Phi_{prompt}) \quad (9)$$

$$k_p = 1/\tau_{prompt}; \; k_d = 1/\tau_{delayed} \quad (10)$$

Supplementary Tables and Figures

Table S1. Photophysical data of PyDCN-PXZ and PyDCN-DMAC in doped films.[a]

	PyDCN-PXZ	PyDCN-DMAC
$\boldsymbol{\Phi}_{\mathbf{PL}}$ **(%)**	89.6	82.8
$\boldsymbol{R}_{\mathbf{delayed}}$	63.6	61.9
$\boldsymbol{\Phi}_{\mathbf{prompt}}$ **(%)**	32.7	31.5
$\boldsymbol{\Phi}_{\mathbf{delayed}}$ **(%)**	56.9	51.3
$\boldsymbol{\Phi}_{\mathbf{IC}}$ **(%)**	3.7	6.5
$\boldsymbol{\Phi}_{\mathbf{ISC}}$ **(%)**	63.6	62.0
$\boldsymbol{\tau}_{\mathbf{prompt}}$ **(ns)**	22.1	14.8
$\boldsymbol{\tau}_{\mathbf{TADF}}$ **(μs)**	6.4	5.6
$\boldsymbol{k}_{\mathbf{F}}$ **(×10^{6}s^{-1})**	14.8	21.3
$\boldsymbol{k}_{\mathbf{IC}}$ **(×10^{6}s^{-1})**	1.7	4.4
$\boldsymbol{k}_{\mathbf{ISC}}$ **(×10^{6}s^{-1})**	28.7	41.9
$\boldsymbol{k}_{\mathbf{RISC}}$ **(×10^{5}s^{-1})**	5.1	4.6

[a] Φ_{PL}, Φ_{prompt}, $\Phi_{delayed}$, Φ_{ISC} represent photoluminescence quantum yield, quantum yield of prompt component, quantum yield of delayed component, intersystem crossing quantum yield, respectively; and k_F, k_{IC}, k_{ISC}, k_{RISC} denote fluorescence decay rate, internal conversion decay rate, intersystem crossing decay rate, and reverse intersystem crossing rate constants, respectively; $R_{delayed}$ represent the ratio of delayed component.

Table S2. EL performance of the white OLEDs based on PyDCNDMAC and representative all-TADF white OLEDs reported in literatures.

EML	η_C [cd A^{-1}]	η_{ext} [%]	CIE (x, y)	Ref
PyDCNDMAC:0.3 wt% PP-PXZ	**44.8**	**18.5**	**(0.38, 0.44)**	**This work**
DMAC-DPS:0.1 wt% CN-QP	48.2	20.1	(0.38, 0.44)	[4]
DMAC-DPS:*X* wt% 4CzTPN-Ph	31.5	13.6	(0.27, 0.33)	[5]
mCP:5CzOXD:4CzPNPh	27	9.9	(0.30, 0.36)	[6]
TXO-PhCz4:0.5 wt% *o*,*o*′-NPh_2	30.2	12.5	(0.38, 0.40)	[7]
TspiroS-TRZ:0.6 wt% DTPA-ADO	51.6	20.5	(0.33, 0.45)	[8]
DCB-BP-SFAC:0.5 wt% TPA-AQ	47.1	19.1	(0.47, 0.45)	[9]
DBFCz-Trz:0.2 wt% BPPZ-DPXZ	95.4	32.8	(0.39, 0.43)	[10]
2tCz2CzBn:1 wt % 1PXZ-BP	/	23.2	(0.39, 0.45)	[11]
*p*tBCzPO2TPTZ:1.5 wt % 4CzTPNBu	52.7	23.6	(0.34, 0.36)	[12]

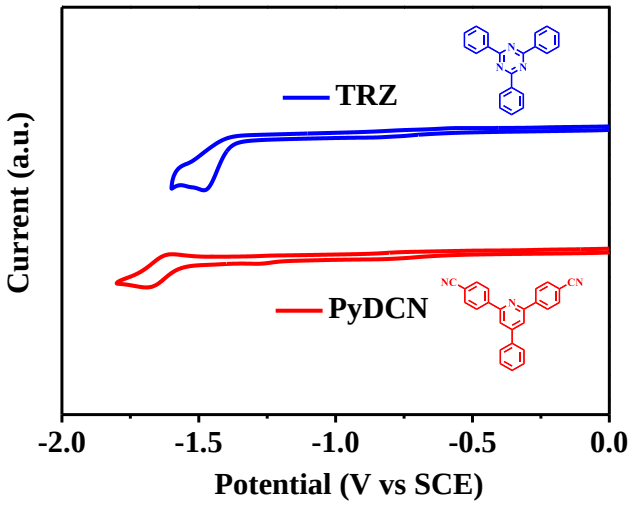

Fig. S1 Comparison of the **c**yclic voltammograms (cathodic scan) between triazine (E_{red}=-1.32 V) and PyDCN (E_{red}=-1.54 V).

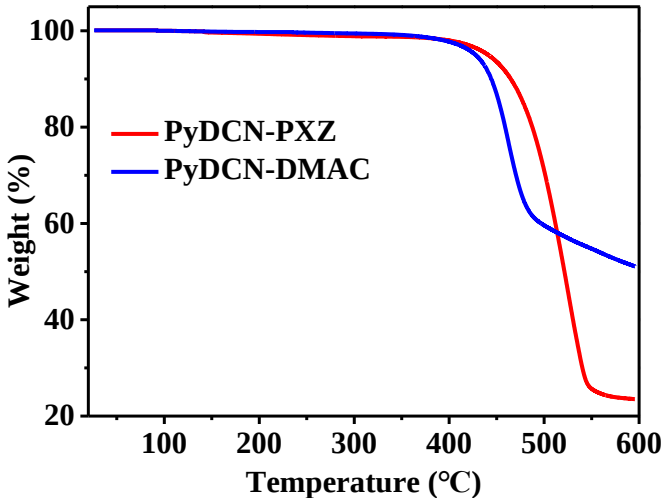

Fig. S2 TGA curves of PyDCN-PXZ and PyDCN-DMAC.

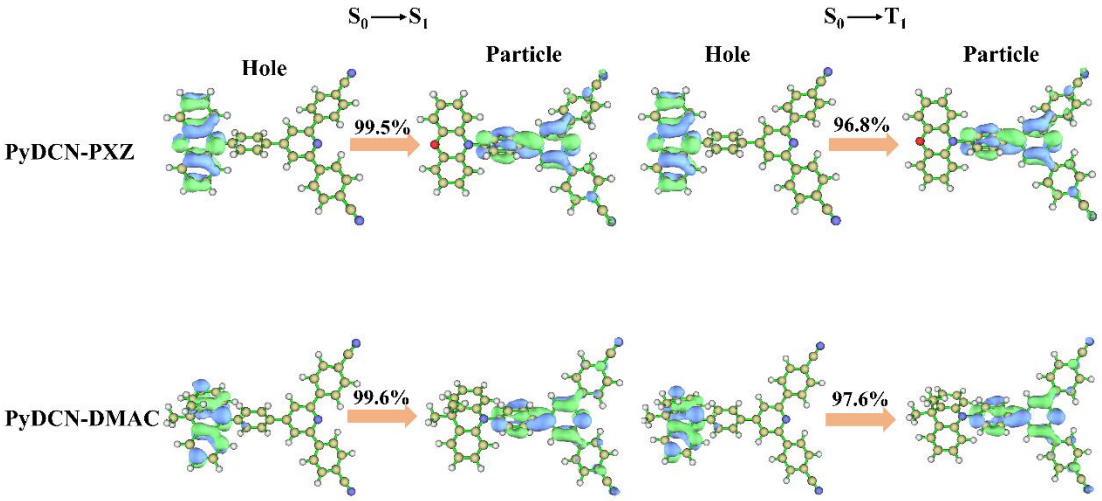

Fig. S3 The natural transition occupied (hole) and unoccupied (particle) orbital distributions and eigenvalues of PyDCN-PXZ and PyDCN-DMAC.

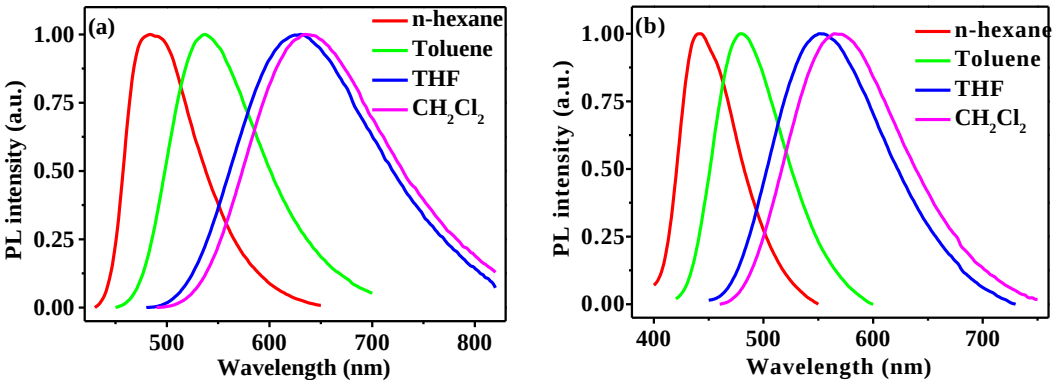

Fig. S4 PL spectra of PyDCN-PXZ (a) and PyDCN-DMAC (b) in different polar solvents.

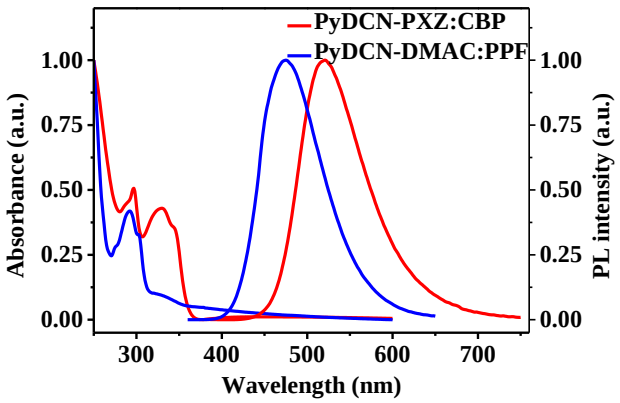

Fig. S5 UV-vis absorption and PL spectra of PyDCN-PXZ and PyDCN-DMAC in solid thin films.

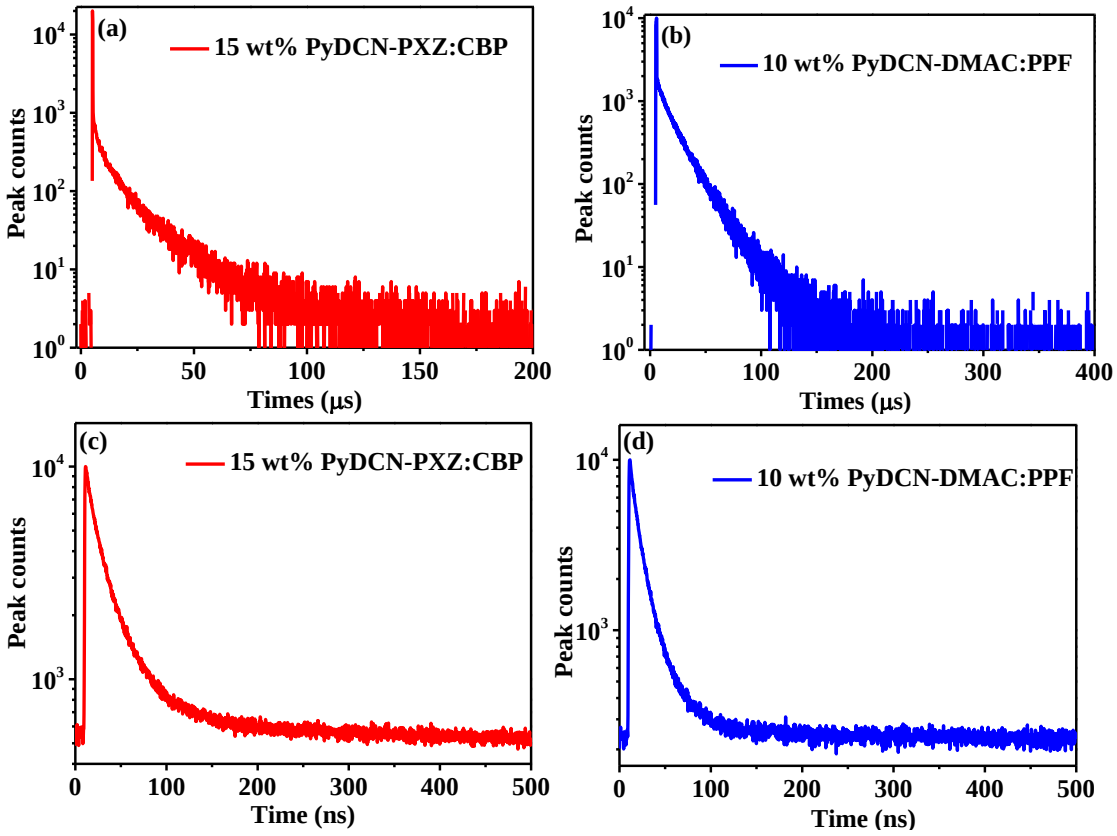

Fig. S6 Transient decay curves measured by multichannel scanning (MCS) method using a 365 nm EPL laser as excitation source for 15 wt% PyDCN-PXZ:CBP film (a) and10 wt% PyDCN-DMAC:PPF film (b), and the decay curves in (c) and (d) were measured by TCSPC technique using a 375 nm picosecond laser as excitation source.

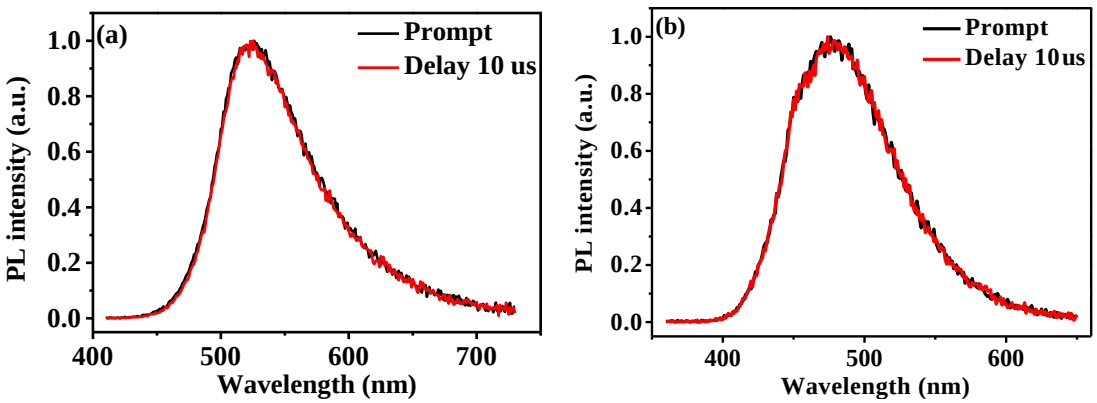

Fig. S7 Delayed fluorescence spectra of PyDCN-PXZ and PyDCN-DMAC in doped films. (a) 15 wt% PyDCN-PXZ:CBP film. (b) 10 wt% PyDCN-DMAC:PPF film.

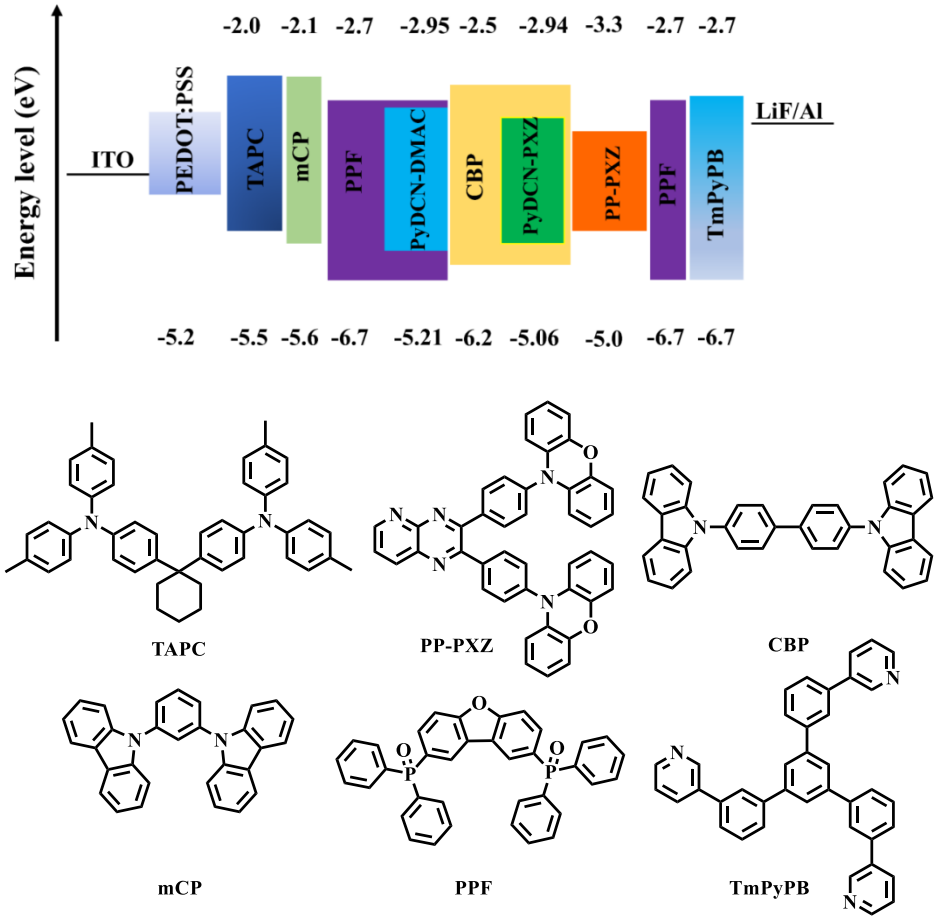

Fig. S8 Chemical structures of related materials and energy level diagram for the TADF OLEDs and all-TADF WOLED.

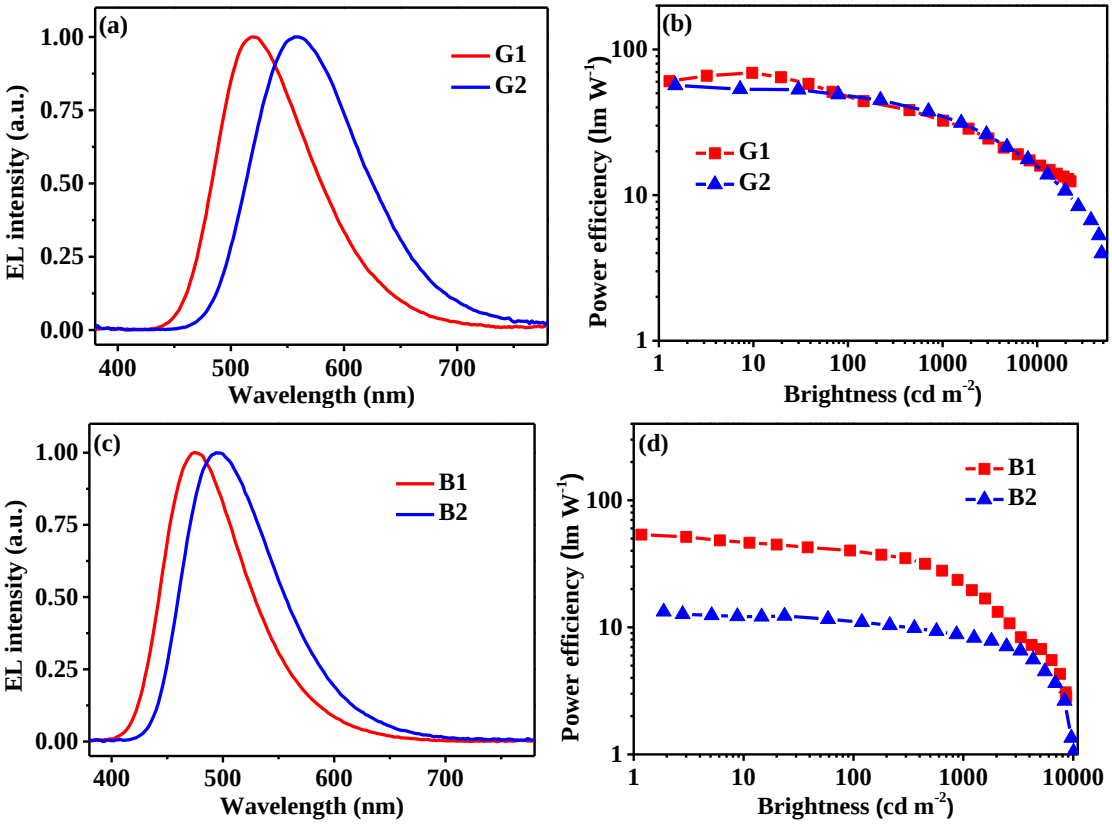

Fig. S9 EL spectra and efficiency curves of PyDCN-PXZ (a, b) and PyDCN-DMAC (c, d) in doped and non-doped OLEDs.

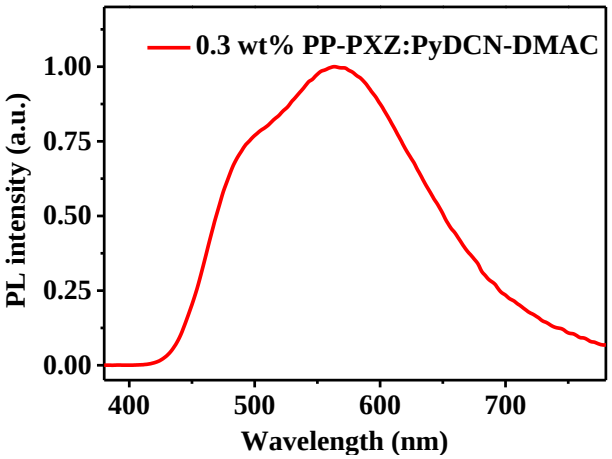

Fig. S10 PL spectrum of the PyDCN-DMAC:PP-PXZ doped film at the same doping concentration (0.3 wt%) as in the emitting layer of the all-TADF white OLED. .

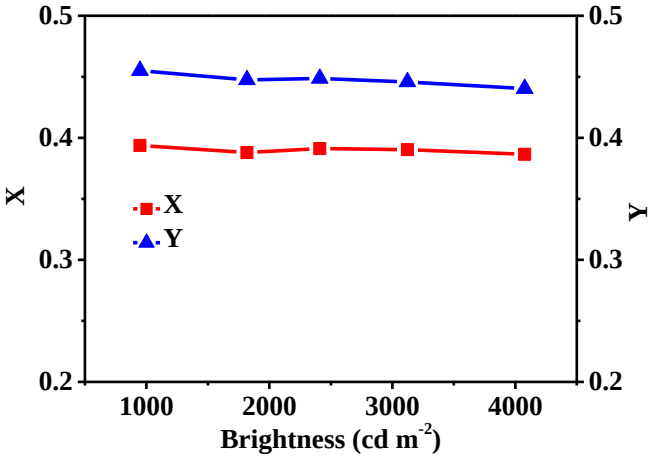

Fig. S11 CIE x and y versus the luminance for the all-TADF white OLED.

References

1 Q. Zhang, H. Kuwabara, W. J. Potscavage, Jr., S. Huang, Y. Hatae, T. Shibata and C. Adachi, Anthraquinone-based intramolecular charge-transfer compounds: computational molecular design, thermally activated delayed fluorescence, and highly efficient red electroluminescence, *J. Am. Chem. Soc*, 2014, **136**, 18070-18081.

2 G. Xie, X. Li, D. Chen, Z. Wang, X. Cai, D. Chen, Y. Li, K. Liu, Y. Cao and S. J. Su, Evaporation- and Solution-Process-Feasible Highly Efficient Thianthrene-9,9',10,10'-Tetraoxide-Based Thermally Activated Delayed Fluorescence Emitters with Reduced Efficiency Roll-Off, *Adv. Mater.*, 2016, **28**, 181-187.

3 H. Uoyama, K. Goushi, K. Shizu, H. Nomura and C. Adachi, Highly efficient organic light-emitting diodes from delayed fluorescence, *Nature*, 2012, **492**, 234-238.

4 T. Huang, D. Liu, D. Li, W. Jiang and J. Jiang, Novel yellow thermally activated delayed fluorescence emitters for highly efficient full-TADF WOLEDs with low driving voltages and remarkable color stability, *New J. Chem.*, 2019, **43**, 13339-13348.

5 W. Luo, T.-T. Wang, X. Chen, K.-N. Tong, W. He, S.-Q. Sun, Y.-J. Zhang, L.-S.

Liao and M.-K. Fung, High-performance organic light-emitting diodes with natural white emission based on thermally activated delayed fluorescence emitters, *J. Mater. Chem. C*, 2020, **8**, 10431-10437.

6 D. Zhang, X. Cao, Q. Wu, M. Zhang, N. Sun, X. Zhang and Y. Tao, Purely organic materials for extremely simple all-TADF white OLEDs: a new carbazole/oxadiazole hybrid material as a dual-role non-doped light blue emitter and highly efficient orange host, *J. Mater. Chem. C*, 2018, **6**, 3675-3682.

7 Y. Chen, S. Li, T. Hu, X. Wei, Z. Li, Y. Liu, J. Liu, R. Wang, Y. Yi, C. Zhao, Y. Wang and P. Wang, Highly efficient white light-emitting diodes with a bi-component emitting layer based on blue and yellow thermally activated delayed fluorescence emitters, *J. Mater. Chem. C*, 2018, **6**, 2951-2956.

8 W. Li, B. Li, X. Cai, L. Gan, Z. Xu, W. Li, K. Liu, D. Chen and S. J. Su, Tri-Spiral Donor for High Efficiency and Versatile Blue Thermally Activated Delayed Fluorescence Materials, *Angew. Chem., Int. Ed.*, 2019, **58**, 11301-11305.

9 H. Chen, H. Liu, P. Shen, J. Zeng, R. Jiang, Y. Fu, Z. Zhao and B. Z. Tang, Efficient Sky-Blue Bipolar Delayed Fluorescence Luminogen for High-Performance Single Emissive Layer WOLEDs, *Adv. Opt. Mater.*, 2021, **9**, 2002019..

10 J. X. Chen, K. Wang, Y. F. Xiao, C. Cao, J. H. Tan, H. Wang, X. C. Fan, J. Yu, F. X. Geng, X. H. Zhang and C. S. Lee, Thermally Activated Delayed Fluorescence Warm White Organic Light Emitting Devices with External Quantum Efficiencies Over 30%, *Adv. Funct. Mater.*, 2021, **31**, 2101647.

11 F. M. Xie, S. J. Zou, Y. Li, L. Y. Lu, R. Yang, X. Y. Zeng, G. H. Zhang, J. Chen and J. X. Tang, Management of Delayed Fluorophor-Sensitized Exciton Harvesting for Stable and Efficient All-Fluorescent White Organic Light-Emitting Diodes, *ACS Appl. Mater. Interfaces*, 2020, **12**, 16736-16742.

12 D. Ding, Z. Wang, C. Li, J. Zhang, C. Duan, Y. Wei and H. Xu, Highly

Efficient and Color-Stable Thermally Activated Delayed Fluorescence White Light-Emitting Diodes Featured with Single-Doped Single Emissive Layers, *Adv. Mater.*, 2020, **32**, 1906950.